Promotion of Deactivated Sintering by Dry-Particle Coating

Michelle Ramlakhan Mohan
Andrx Pharmaceuticals, Inc., Ft. Lauderdale, FL 33314

Rajesh N. Dave and Robert Pfeffer
New Jersey Center for Engineered Particulates, New Jersey Institute of Technology, Newark, NJ 07102

Dry-particle coating was used to examine the feasibility of increasing the sintering temperatures of different particulate materials (hosts) by applying a discrete coating of a highly refractory material (guest). Increasing the sintering temperature reduces the sintering rate of the material, and hence the phenomenon is called "deactivated sintering." Several host particles, such as glass beads, PMMA, γ-alumina, and an alumina–silica composite, were coated with submicron-size silicon carbide in three different dry-particle coating devices: magnetically assisted impaction coating, mechanofusion, and hybridizer. The coated products were characterized using several techniques, including particle-size analysis, SEM, EDX, BET, optical microscopy, and dilatometry studies to compare the coating performance of each device. By coating the host particles with silicon carbide, it was possible to appreciably increase the sintering temperatures of all four of the particulate host materials. Simple phenomenological sintering models based on volume diffusion for crystalline materials and viscous flow for amorphous materials were combined with dilatometry data to explain the phenomenon of deactivated sintering. For γ-alumina, there was a significant reduction in the effective diffusivity due to the addition of a surface coating of SiC, whereas for SiC-coated glass beads and PMMA, an increase in the effective viscosity was postulated as the cause of deactivated sintering.

Introduction

When two particles in mutual contact form a system that is not thermodynamically stable, that is, when the total surface free energy is not a minimum, the two particles, if left for a period of time, begin to bond together (Kuczynski, 1949a). Bonding occurs in order to decrease the total surface area even though the particles are at temperatures lower than their melting temperature. This phenomenon of the bonding of two or more particles with the application of heat at temperatures below the melting point of the particles is called sintering. At the minimum sintering temperature, T_s (where sintering just begins), two phenomena are observed to occur simultaneously (Bonis and Hausner, 1964). First, the contact area of the two particles (of diameter 2R) touching each other grows, that is, the neck (of size 2x) between the particles increases, as shown in Figure 1. Second, loose powder aggregates or compacts become denser by a decrease in the distance between the centers of the particles. This results in an overall decrease in the total volume of the sample, and an approach to the theoretical density of the material.

The first, and by now, classic experiments on the mechanism of material transport in sintering powders were presented by Kuczynski (1949a and 1949b). His studies examined the driving force of sintering for metals and glass. Several investigators have gone on to present compiled works on the sintering behavior of ceramics and polymers, for instance, Coble (1961). Studies also have been conducted on the sintering behavior of a two-component system, where one material is mixed together with a very small amount by weight of another material to enhance the sintering rate of the first material. This is referred to in the literature as "activated sintering" whereby the minimum sintering temperature of the ma-

Correspondence concerning this article should be addressed to R. Pfeffer.

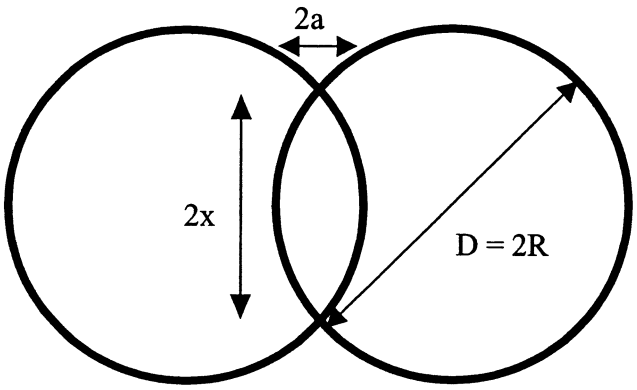

Figure 1. Neck growth during sintering for two spheres of similar size.

terial is lowered by the addition of a monolayer of a second component. For metals, nickel-activated sintering of tungsten has been reported (German, 1984). The effect was pronounced, as normally tungsten sinters at temperatures around 2,700°C to get near the theoretical (maximum) density. However, with the addition of 0.01 wt % nickel, the theoretical density of tungsten was obtained at about 1,400°C. For the ceramic analogy, activated sintering of beryllia was found to occur with small additions of calcium oxide. With a calcium oxide addition to beryllia, the approximate temperature required to achieve high density was lowered by several hundred degrees centigrade (Bonis and Hausner, 1964).

Activated sintering has also been used to describe the formation of composites whereby a low concentration of one material is added to another material to promote grain boundary segregation so as to increase diffusion rates. The increase in diffusion gives rise to faster rates of sintering, hence a lowering of the sintering temperature of the material (Johnson and German, 1996; Panin et al., 1996; Luo et al., 1999). Activated sintering of materials by a surface coating or the formation of uniquely tailored composites is thoroughly discussed in the literature and plays an important role in many applications.

There is, however, no information on two-component systems for "deactivated sintering." Deactivated sintering can be defined as a process whereby the surface of particles is coated with a monolayer of another material to delay and reduce the sintering of the material, hence causing an increase in the minimum sintering temperature. The delay in sintering might be caused by an increase in the activation energy of the system, which gives rise to slower rates of diffusion. The question then arises as to the importance and application of increasing the sintering temperature of materials. There are several applications in which deactivated sintering can be useful.

One such application is in fluidized beds used in the petrochemical and many other industries. In these fluidized beds, the use of a catalytic material is usually confined to a specific temperature range, which controls the product yield. Temperature control within this range is very important, as an unmonitored increase in temperature will cause the catalytic material to begin to soften and fuse together (sinter). As this occurs, the sizes of the particles change as they begin to aggregate. To keep the fluidized bed active or "alive," quick adjustments must be made to the gas velocity of the process (Siegell, 1984). If this is not done in time, the bed can become inactive (defluidized) or "dead," resulting in a significant loss of time and money. The application of a surface coating to promote deactivated sintering of these materials can allow beds to be run at higher temperatures without fear of defluidization by sintering. Deactivated sintering technology can also be expanded to include glass and polymeric particles used in fluidized-bed applications, where defluidization due to the sticking of particles to form large agglomerates is of a primary concern.

A second possible application under investigation is in the coating of polymeric materials. Many polymeric materials are used for the construction of spacecraft, but in low-orbit space flight, these polymers are subjected to destructive components, such as ionizing radiation (keV electrons and MeV protons), vacuum ultraviolet photons, and extreme temperatures. As a result, these materials suffer rapid erosion and surface roughening (Houdayer et al., 1997). The polymers may undergo an irreversible degradation of their physical properties, such as optical, thermal, and electrical, for which they have been designed specifically. It has been reported that a thin inorganic coating on the polymer materials can protect the surfaces to prevent this degradation from occurring. Therefore, coating the surface of a material to promote deactivated sintering can also provide a protection layer to prevent the degradation of polymeric materials at elevated temperatures.

To understand the mechanism of sintering, Frenkel (1945) made a first attempt to develop a theory of sintering. In this study, it was assumed that the process was due to a slow deformation of the crystalline particles under the influence of surface tension, which reduces to a viscous flow. Kuczynski (1949a) discussed several possible mechanisms of sintering and, unlike other researchers, presented experimental data to define the predominant mechanism. Kuczynski (1949a) defined four possible mechanisms for the transport of material to form a bond between two particles, surface diffusion, volume diffusion, viscous flow, and evaporation.

Surface and volume diffusion are produced by the motion of atoms from one place to an adjacent place in the lattice structure. This occurs from regions of high density to more porous sections of the material. Surface diffusion has been reported to be only important during the initial stage of sintering and is caused by the initial adhesion between the particles. Surface diffusion cannot promote substantial densification, and volume diffusion is chiefly responsible for densification. Surface and volume diffusion mechanisms are the predominant mechanisms of sintering in crystalline and metallic particles.

Unlike diffusion mechanisms of sintering, sintering by viscous flow involves the movement of lattice planes from high- to low-vacancy concentration areas, which is initiated by the effects of surface tension or external forces (Tardos et al., 1984). Sintering by a viscous flow mechanism is the predominant means of material transport for the sintering of polymeric, glassy, and nonmetallic materials. The evaporation or condensation mechanism of sintering involves transport in the vapor phase. This is considered the least important mechanism of sintering.

Johnson and German (1996) expanded the volume diffusion mechanism presented by Kuczynski (1949a) and the three stages presented by Coble (1961) to derive a theoretical model for activated solid–solid sintering. Activated sintering described by Johnson and German (1996) involved the formation of composites with small additions of transition elements to metals aimed at accelerating the sintering rate by decreasing the activation energy for diffusion at the grain boundary, resulting in higher diffusion rates. The three stages used to define sintering in this model are the initial, the intermediate, and the final stage. In the initial stage, there is neck growth and densification as the distance between the centers of particles in contact decreases. After some time, when the neck region has decreased sufficiently, the equations for initial sintering are no longer valid. The intermediate stage involves the rounding and smoothing of the interconnective pores at the grain boundaries. In the final stage, as densification continues, the pores begin to close and the microstructure of the particles is then defined by spherical pores at the grain boundaries (Coble, 1958).

We have used dry particle coating (Alonso et al., 1988, 1989a,b; Ramlakhan et al., 2000; Pfeffer et al., 2001; Watano et al., 2000) to change the properties of a variety of host particles to promote deactivated sintering, that is, a reduction in sintering rate and an increase in the minimum sintering temperature of particulate materials. Several host particles are coated with small amounts of the highly refractory SiC (guest particles) in three different dry particle–coating devices. The three devices used are the magnetically assisted impaction coater (Hendrickson et al., 1997; Singh et al., 1997), mechanofusion (Tanno, 1990; Yokoyama et al., 1987; Naito et al., 1993), and the hybridizer (Honda et al., 1991, 1994; Ishizaka et al., 1988). The host particles chosen are PMMA, glass beads, a high purity γ-alumina, and a composite of alumina and silica. The properties of these particles as well as the properties of the SiC guest particles are given in Table 1.

Glass beads and PMMA are chosen as host particles, as they are perfectly spherical, nonporous, and can be coated quite uniformly with silicon carbide guest particles. They are excellent model systems to study deactivated sintering by the viscous flow mechanism. Alumina–silica and γ-alumina are chosen as host particles, as they represent true systems of interest, in that they are porous particles, irregular in shape and, most importantly, are commercially available catalytic support materials. These particles sinter predominately by volume diffusion. SiC is chosen as the guest particle for all of the host particles because it has a very high melting point, and thus a corresponding high sintering point, which is much higher than that of the host particles.

Table 1. Properties of Host and Guest Particles

Samples	Density (g/cm^3)	Mean Size (μm)	Description
PMMA (host)	1.19	200	Spherical, smooth, nonporous
Glass beads (host)	2.5	300	Spherical, smooth, nonporous
Alumina–silica (host)	3.6	40	Irregular, porous
Alumina (host)	3.9	80	Irregular, porous
SiC (guest)	3.2	0.5	Irregular

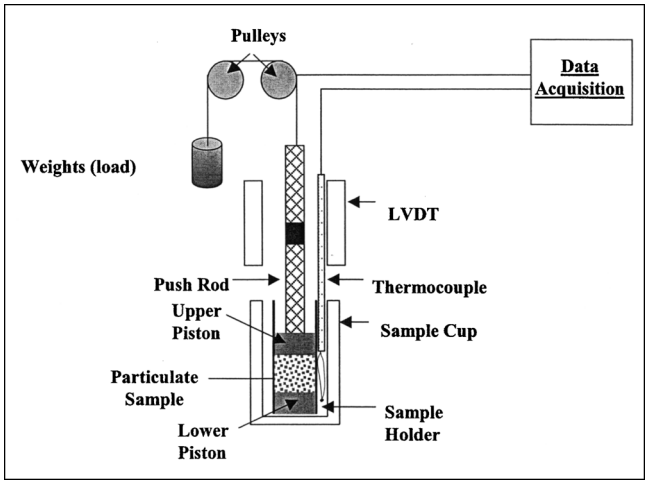

Figure 2. Modified vertical dilatometer.

In this study the coated products are characterized to compare the coating performance of each device, and to examine the changes in the sintering rates of the materials for the promotion of deactivated sintering. Several characterization techniques are used to fulfill these objectives. Particle-size analysis (API Aerosizer) is conducted to measure changes in the mean size of the materials after processing. A scanning electron microscope (SEM) and an optical microscope are used to examine the surface morphology and neck growth of the sintered particles. EDX mapping is used to show the presence of silicon (from silicon carbide) on the surface of the host particles. BET surface area analysis is used to measure changes in the surface area and pore size of the porous host particles after coating and after sintering. A modified vertical dilatometer (Figure 2) is used to measure the sintering temperatures of the materials (Compo et al., 1984). The samples, before and after being coated, are heated in the dilatometer, and the expansion/contraction of the material as a function of temperature is plotted. From these curves, the minimum sintering temperature, defined as the lowest temperature at which the surface of the particles just begin to soften and the sintering process begins (represented by a sharp drop in the dilation vs. temperature curve), is obtained (Compo et al., 1987).

Simple phenomenological sintering models based on volume diffusion for crystalline materials and viscous flow for amorphous materials (Kuczynski, 1949a; Coble, 1958; Johnson and German, 1996; and Tardos et al., 1984), combined with dilatometer data, are used to explain the phenomenon of deactivated sintering. Thus, we propose that there is a significant reduction in the diffusion rate (effective diffusivity) due to the addition of a surface layer of SiC at the initial stages of sintering for the alumina and alumina–silica samples. For SiC-coated glasses and polymers, an increase in the effective viscosity of the particles is postulated as the mechanism of deactivated sintering. A much more rigorous theoretical analysis of the process of deactivated sintering, taking into account the intrusion of the coated particles into the "viscous" host particles, and an introduction to the concept of the latent time of deactivation, will be presented in a second article in preparation.

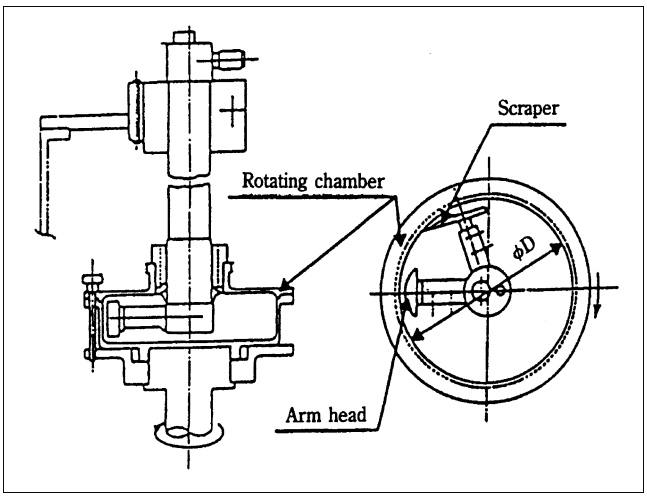

Figure 3. Mechanofusion process (Yokoyama et al., 1987; Pfeffer et al., 2001).

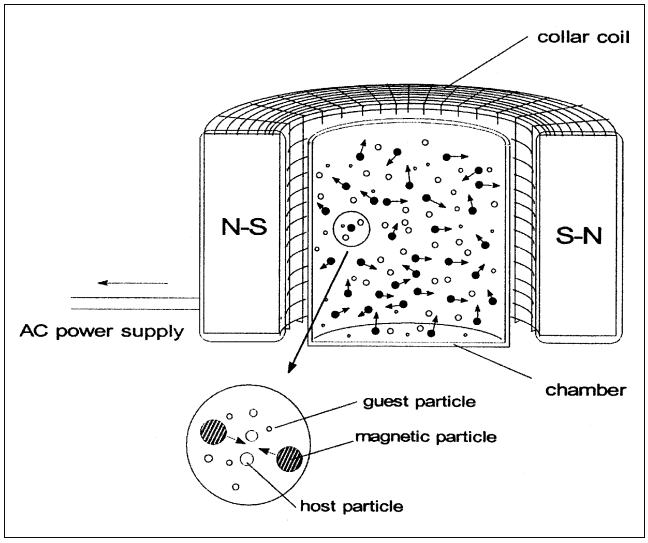

Figure 5. MAIC process (Singh et al., 1997; Pfeffer et al., 2001).

Experimental Studies

Measured amounts of host and guest particles are processed by mechanofusion (henceforth called MF), the hybridizer (henceforth called HB) and the magnetically assisted impaction coater (henceforth called MAIC). MF, HB, and MAIC are shown in Figures 3, 4, and 5, respectively. A detailed description of how each of these devices generates the necessary mechanical forces to coat the guest particles onto the surface of the host particles is outside the scope of this article, but can be found in Pfeffer et al., 2001. The mass percentage of guest particles to be used in an experiment is usually calculated based on the assumption of 100% surface coverage of the host particles with a monolayer of guest particles. The assumptions for the calculation are that all guest particles are of the same size, the host and guest particles are spherical, and the guest particles do not undergo deformation.

From these assumptions, the number of guest particles, N, required to coat one host particle with a continuous monolayer is derived from the following simple expression

$$N = \frac{S_{D+d}}{S_d} = \frac{\pi(D+d)^2}{\frac{\pi d^2}{4}} = \frac{4(D+d)^2}{d^2}, \qquad (1)$$

where S_d is the cross-sectional area of a guest particle, D is the diameter of a host particle, d is the diameter of a guest particle, and S_{D+d} is the surface area of the sphere with diameter $(D+d)$. Therefore, for any give batch size, based on 100% surface coverage, the weight percentage of guest particles to be used is

$$G(\text{wt. }\%) = \frac{\text{Mass of guest}}{\text{Total mass of system}} = \frac{\left(N \times d^3 \times \rho_d\right)}{\left(D^3 \times \rho_D\right) + \left(N \times d^3 \times \rho_d\right)} \times 100, \qquad (2)$$

where N is given by Eq. 1, ρ_D is the density of the host material, and ρ_d is the density of the guest material.

For MAIC, which uses magnetic particles under the influence of an oscillating magnetic field to "fluidize" and coat the host particles, a measured amount of magnets (barium ferrite, coated with polystyrene, 1–2 mm size) is also placed in with the host and guest particles, at a predefined mass ratio of magnet to host particles (usually 2). The mass percentages of guest particles used in each experiment are listed in Tables 2 to 4. The processing times, batch size (amount of

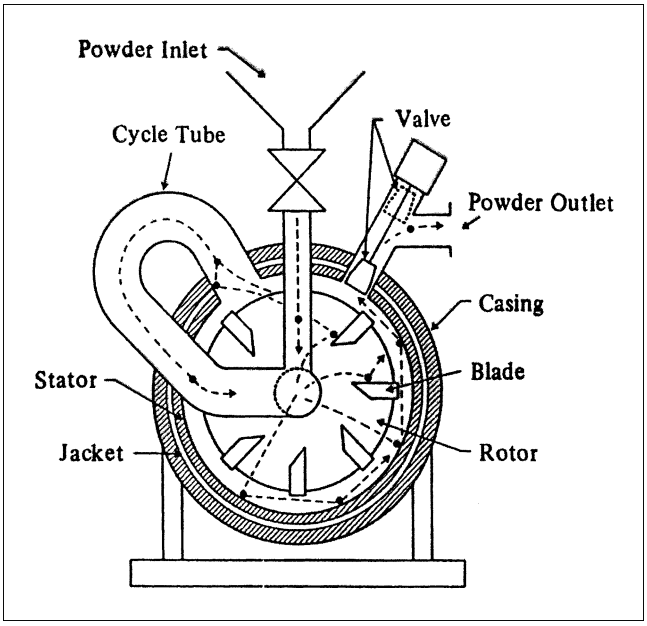

Figure 4. Hybridizer process (Ishizaka et al., 1988; Pfeffer et al., 2001).

Table 2. Operating Parameters for MAIC

Samples	Processing Time (min)	Guest wt. %	Total Batch Size (g)
PMMA	10	3	10
Glass beads	10	0.8, 8	10
Alumina	10	2	10
Alumina–silica	2.5, 5, 10	2	10

Table 3. Operating Parameters for Mechanofusion (600 rpm)

Samples	Processing Time (min)	Guest wt. %	Total Batch Size (g)
PMMA	10	3	50
Glass beads	10	0.8, 8	100
Alumina	10, 20	2	50
Alumina–silica	N/A	N/A	N/A

material processed in each device), and rotational speeds at which the devices are operated, are also listed in Tables 2 to 4.

The load on the dilatometer in all the experiments with PMMA, glass beads, high-purity alumina, and alumina–silica was kept constant at 35 g, and the heating rate was set at 5°C/min, except when using PMMA, where the heating rate was set at 2.5°C/min.

Results and Discussion

PMMA

The glass transition temperature of uncoated PMMA is approximately 105°C (Lide, 1998), and the softening temperature is approximately 110°C. The weight percentage of guest particles used is 3%, and is based on the assumption that 100% of the surface of the PMMA host particle is covered with a monolayer of SiC (Eq. 2). The coated samples obtained from the three devices, as well as uncoated PMMA, were heated to different temperatures in the dilatometer to examine the degree of sintering as a function of temperature. The temperatures used were 130°C and 150°C, respectively. Optical micrographs of the uncoated samples and the coated samples, at room temperature are shown in Figures 6a to 6d. At 130°C, the uncoated sample showed beginning signs of sintering, whereas the coated samples from all three devices showed no signs of neck growth or fusion between particles. Optical micrographs for the uncoated and the MAIC-coated sample at 130°C are shown in Figures 7a and 7b, respectively.

At 150°C, the uncoated PMMA was a solid fused mass (Figure 8a). The MAIC-, MF-, and HB-coated samples showed initial signs of sintering at 150°C (Figures 8b to 8d),

Table 4. Operating Parameters for Hybridizer (6,000 rpm)

Samples	Processing Time (min)	Guest wt. %	Total Batch Size (g)
PMMA	5	3	20
Glass beads	N/A	N/A	N/A
Alumina	2	2	20
Alumina–silica	2	2	50

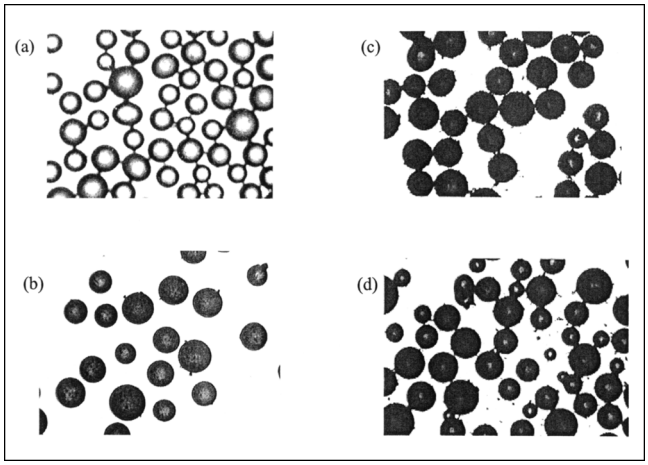

Figure 6. Optical micrographs of (a) uncoated PMMA, (b) HB-coated PMMA, (c) MAIC-coated PMMA, and (d) MF-coated PMMA, at room temperature.

but were mainly loose individual particles. SEM micrographs of uncoated PMMA and PMMA coated in the MAIC, MF, and HB at room temperature are shown in Figures 9a to 9d, respectively. As seen in Figures 9b to 9d, the samples processed in all three devices were coated with SiC; the MAIC and the MF samples were discretely covered, while the HB samples were more densely coated. The shrinkage as a function of temperature for the uncoated as well as the coated samples heated to 150°C in the dilatometer is shown in Figure 10. The percent shrinkage is defined as

$$\text{Shrinkage } \% = 100\left\{\frac{\left[\frac{\Delta L}{L_0}\times L_0\right]_{T=T_0} - \left[\frac{\Delta L}{L_0}\times L_0\right]_{T=T}}{L_0}\right\}, \tag{3}$$

and $\Delta L/L_0$ at different temperatures is obtained directly from the dilatometer measurements. As seen in Figure 10, when heated to 150°C, there was a much larger shrinkage of the uncoated PMMA sample than the coated samples.

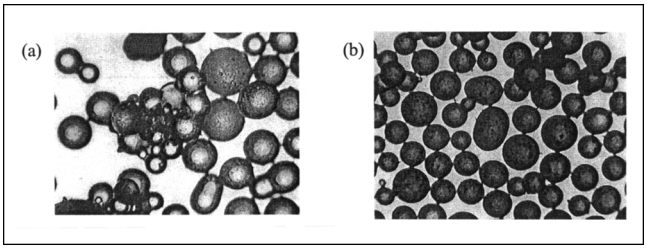

Figure 7. Optical micrographs of (a) uncoated PMMA and (b) MAIC-coated PMMA, heated to 130°C in the dilatometer.

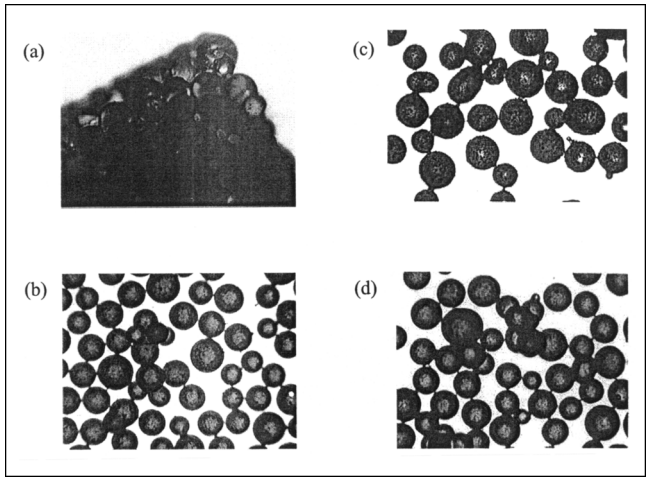

Figure 8. Optical micrographs of (a) uncoated PMMA, (b) HB-coated PMMA, (c) MAIC-coated PMMA, and (d) MF-coated PMMA, heated to 150°C in the dilatometer.

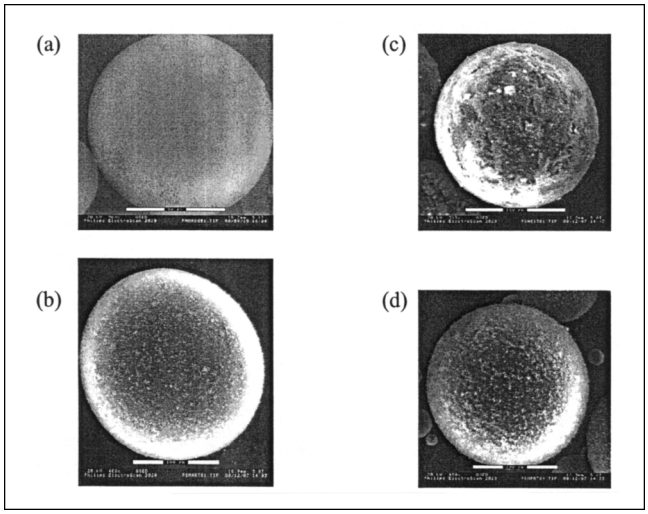

Figure 9. SEM micrographs of (a) uncoated PMMA, (b) MAIC-coated PMMA, (c) HB-coated PMMA, and (d) MF-coated PMMA, at room temperature.

Glass beads

Glass-bead samples processed in the HB were crushed due to their brittle nature, so coating experiments could not be continued. Coated samples were prepared in MAIC and MF using two different weight percent of guest particles, 0.8% and 8%, respectively. This was done to examine the degree of sintering as a function of guest weight percentage. The amount of guest particles required to cover 100% of the surface of a glass bead with a monolayer, from Eq. 2, is 0.8 wt. % of SiC. Thus, the samples prepared with 8% SiC were much more heavily coated. The coated samples, as well as the uncoated glass beads, were heated in the dilatometer to 600, 700 and 800°C, respectively. The minimum sintering temperature of uncoated glass beads is approximately 575°C (Tardos et al., 1984).

Optical micrographs of the uncoated, 0.8 wt. % and 8 wt. % coated samples in MAIC at room temperature are shown in Figure 11. At 600°C (Figure 12a), the uncoated sample showed beginning signs of sintering with an increase in contact (neck) area. This increase in contact area was not visible with the 0.8 and 8 wt. % guest coated samples (Figures 12b and 12c). At 700°C, most of the uncoated sample was fused together, whereas the 0.8 and 8 wt. % coated samples remained as individual particles, as shown in Figures 13a to 13c. At 800°C, both the uncoated and the 0.8 wt. % coated samples were completely fused, as shown in Figures 14a and

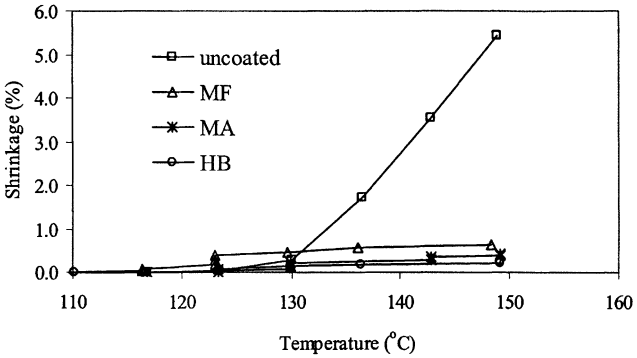

Figure 10. Shrinkage of PMMA samples heated to 150°C in the dilatometer.

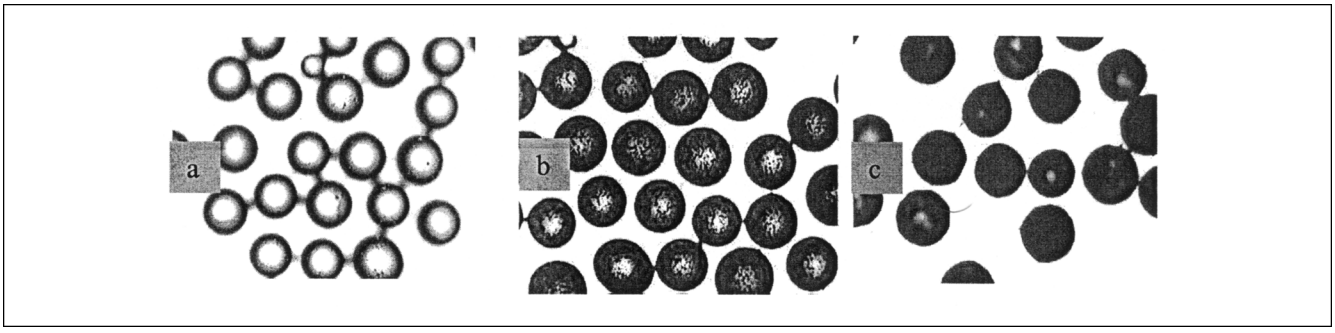

Figure 11. Optical micrographs of (a) uncoated glass beads, (b) 0.8 wt. % SiC-coated glass beads, and (c) 8 wt. % SiC-coated glass beads, at room temperature.

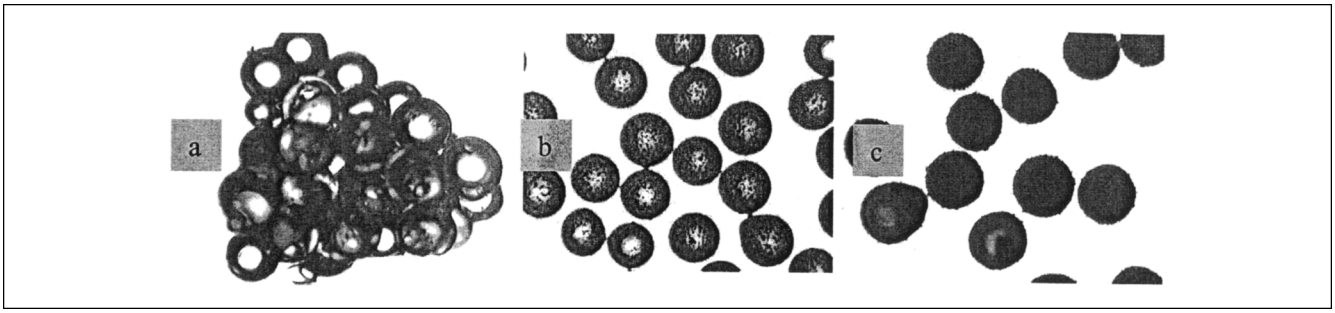

Figure 12. Optical micrographs of (a) uncoated glass beads, (b) 0.8 wt. % SiC-coated glass beads, and (c) 8 wt. % SiC-coated glass beads, heated in the dilatometer to 600°C.

14b. However, the 8 wt. % guest coated sample still remained mostly as individual particles, with just a small amount of neck growth visible (Figure 14c). Similar results were obtained for the MF processed particles. This clearly showed that a thicker, more continuous coverage of coating results in better promotion of deactivated sintering.

SEM micrographs of glass beads uncoated and coated in the MAIC (10 min with 0.8 wt. % of SiC) are shown in Figures 15a and 15b, respectively. A much thicker, relatively uniform coating of SiC is clearly visible for the 8 wt. % of the SiC-coated sample (Figure 15c). Similar results were obtained when MF was used as the dry coating process.

High-purity γ-alumina

SEM micrographs of the uncoated and the MF-coated samples are shown in Figure 16. EDX mappings of silicon on the surface of the coated samples obtained from the three devices are shown in Figure 17. The weight percentage of guest particles used in the coating devices was 2%, based on Eq. 2. However, it is clear from Figures 16 and 17 that the host is not "film" coated, that is, the surface is coated discretely with SiC rather than uniformly. It is also probable that our dry-coating devices were not able to disperse all of the SiC powder into individual particles, so that some of the coating may consist of larger agglomerates rather than a monolayer of primary particles.

The BET measured specific surface area and the average pore size of the uncoated and coated samples before sintering are shown in Figures 18 and 19, respectively. Placing a discrete coating of SiC on alumina did not decrease the surface area or reduce the average pore size by clogging and blocking the pores, which were initial concerns.

The dilatometry results of contraction, $\Delta L/L_0$, as a function of temperature for uncoated alumina, and alumina processed by MAIC (5 min), MF (10 min, 600 rpm), and HB (2 min, 6,000 rpm) heated to 1,550°C are shown in Figure 20. Where the greatest change in gradient occurs for each curve is a measure of the minimum sintering temperature. It can be seen that all of the coated samples had a higher minimum sintering temperature than the uncoated sample, with the MF sample showing the highest. The percent shrinkage as a function of temperature is shown in Figure 21. The uncoated samples had an overall shrinkage of about 9%, while the coated samples had an overall shrinkage of less than 3%. The mechanofusion samples had the lowest shrinkage of about 0.75%. SEM micrographs (Figures 22a to 22d) of the samples, after being heated to 1,550°C, confirmed the dilatometry results, by showing fully sintered uncoated particles and unsintered or partially sintered coated samples obtained from the HB, MAIC, and MF.

The specific surface area of the uncoated and coated samples after sintering is shown in Figure 23. As expected, after being heated to 1,550°C in the dilatometer, there was a drastic reduction in the specific surface area due to the phase change from γ- to α-alumina. A closer look at the phase transformation was obtained by heating the uncoated and the MAIC-coated samples to 800, 1,000 and 1,250°C, in the dilatometer and measuring the specific surface area. The specific surface area of the uncoated and coated samples as a

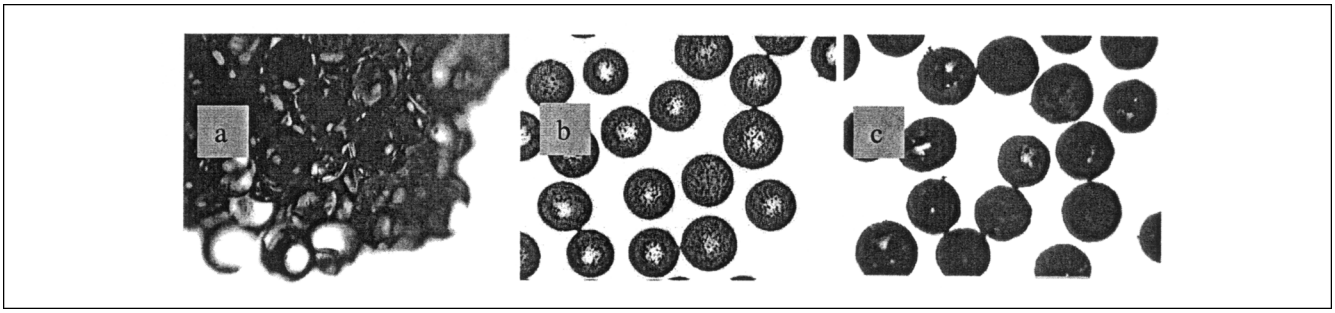

Figure 13. Optical micrographs of (a) uncoated glass beads, (b) 0.8 wt. % SiC-coated glass beads, and (c) 8 wt. % SiC-coated glass beads, heated in the dilatometer to 700°C.

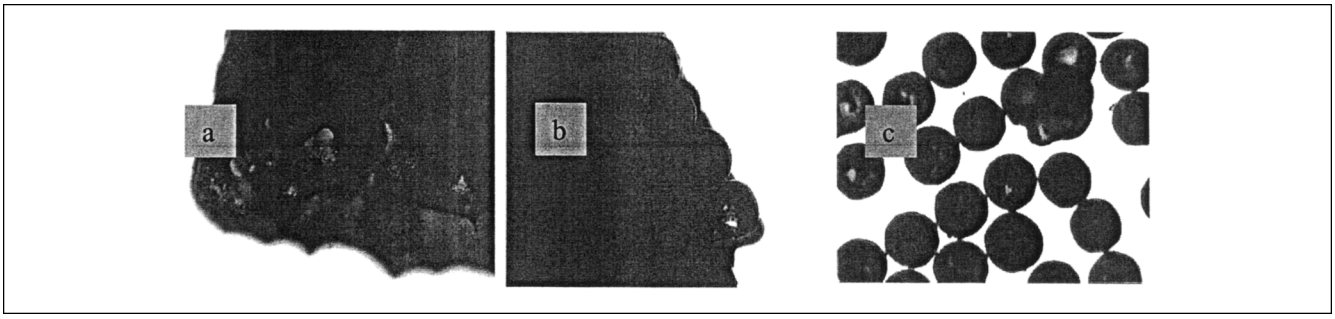

Figure 14. Optical micrographs of (a) uncoated glass beads, (b) 0.8 wt. % SiC-coated glass beads, and (c) 8 wt. % SiC-coated glass beads, heated in the dilatometer to 800°C.

function of temperature is shown in Figure 24. It can be seen that within experimental error, the specific surface area of the uncoated and coated samples appears to be the same. Moreover, the phase change from γ- to α-alumina takes place around 1,000°C, much lower than the sintering temperature of the uncoated material. We conclude that high-purity γ-alumina coated with SiC promotes deactivated sintering at elevated temperatures, that is, prevents softening of the surface and agglomeration due to sintering. However, the reduction in surface area due to the phase change from γ to α makes the material unattractive as a catalytic support at high temperatures.

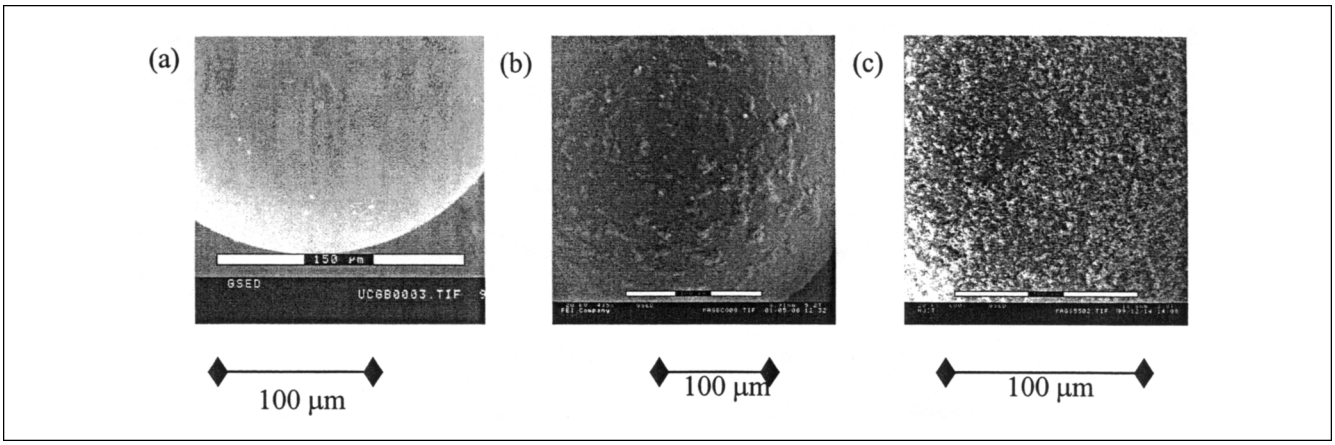

Figure 15. SEM micrographs of (a) uncoated glass beads, (b) 0.8 wt. % SiC-coated glass beads, and (c) 8 wt. % SiC-coated glass beads, at room temperature.

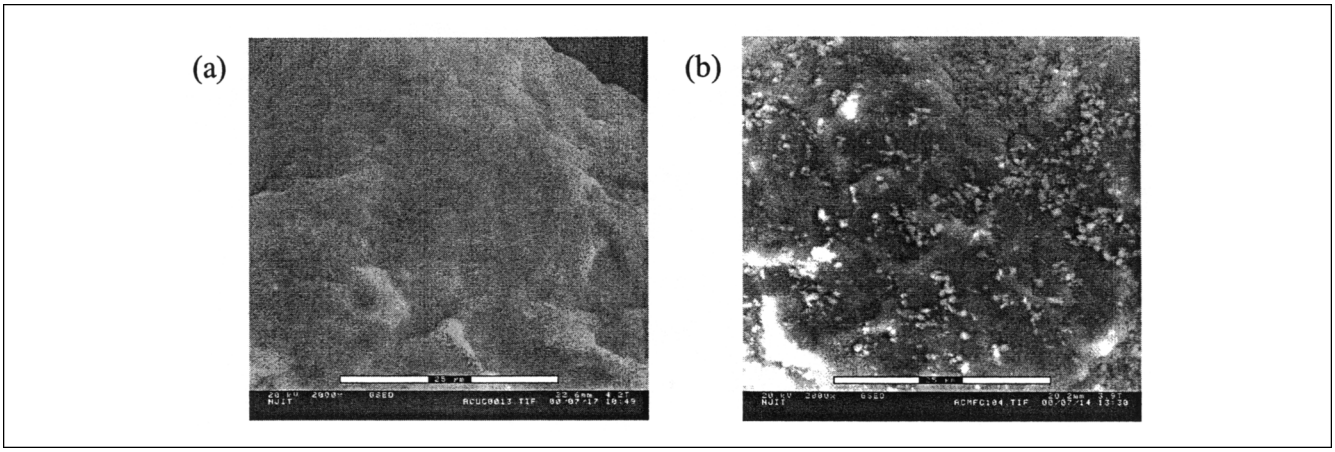

Figure 16. SEM micrographs of (a) alumina uncoated and (b) alumina coated for 10 min in the MF, at room temperature.

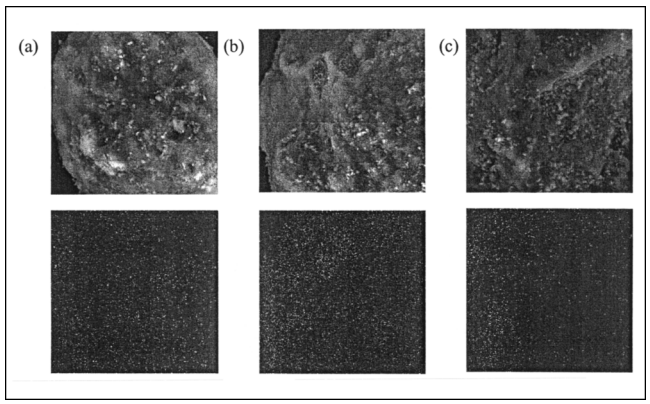

Figure 17. SEM micrographs with corresponding EDX mapping of silicon for (a) HB-coated alumina (2 min, 6,000 rpm), (b) MAIC-coated alumina (5 min), and (c) MF-coated alumina (10 min, 600 rpm).

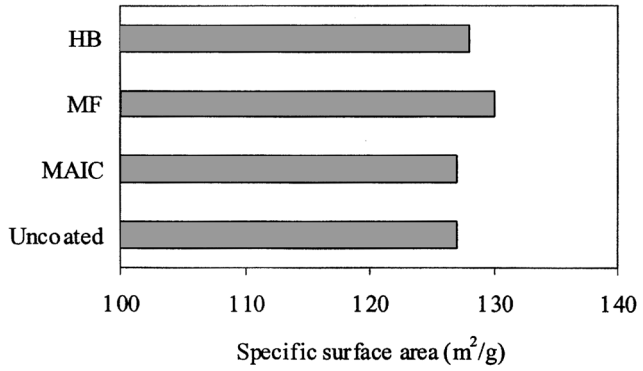

Figure 18. BET-specific surface area at room temperature.

Alumina – Silica

The alumina–silica catalytic support was not run in MF, as it requires a large batch size, which was not possible due to the small amount of material that we had available. The volume–mean particle size of the coated samples from the MAIC and HB, as well as the uncoated sample, is shown in Figure 25. The figure shows that there was significant size reduction due to attrition in all of the processed samples, with the largest attrition occurring in the HB. A large change in the mean particle size is undesirable, since this will not only affect the dilatometry results, but can also affect the function of the catalytic support material.

SEM photographs of the MAIC samples showed that the surface coverage of the sample processed for 10 min was about 50%, compared to 11% and 14% for the samples processed for 2.5 and 5 min, respectively. Although a large surface coverage is desirable to help promote deactivated sintering, the desired coating for these particles should not be so large as to reduce the surface area of the catalytic material by clogging the pores. Hence, only dilatometry analysis of the samples processed for 2.5 and 5 min, as well as the uncoated support, was conducted.

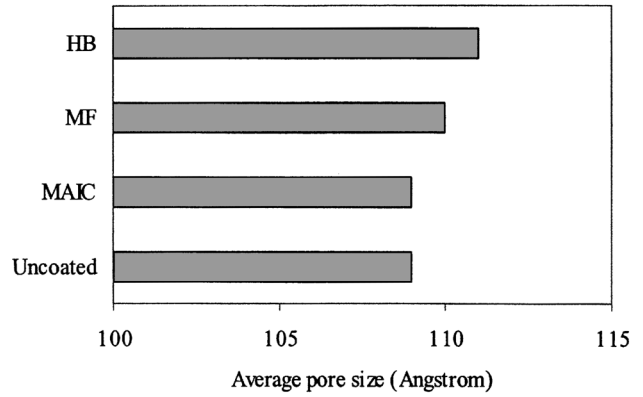

Figure 19. BET average pore size at room temperature.

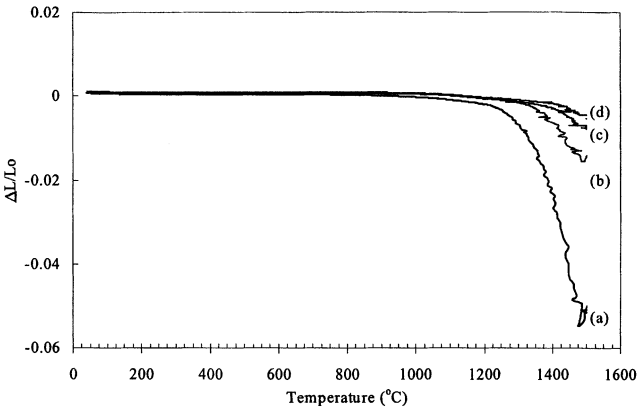

Figure 20. Elongation–contraction vs. temperature for (a) uncoated alumina, (b) alumina coated in MAIC (5 min), (c) alumina-coated HB (2 min, 6,000 rpm), and (d) alumina coated in MF (10 min, 600 rpm).

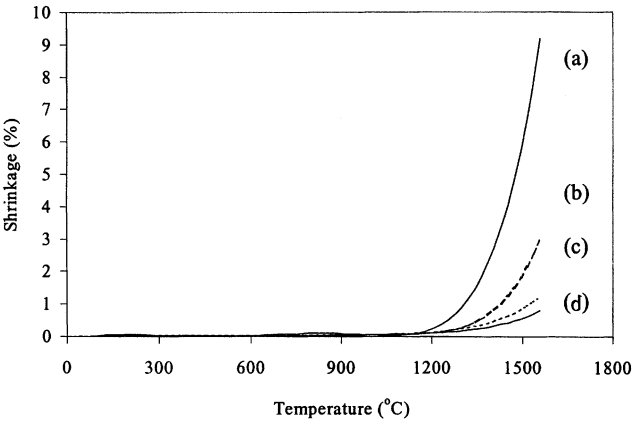

Figure 21. Shrinkage as a function of temperature for (a) uncoated alumina, (b) alumina coated in MAIC (5 min), (c) alumina-coated HB (2 min, 6,000 rpm), and (d) alumina coated in MF (10 min, 600 rpm).

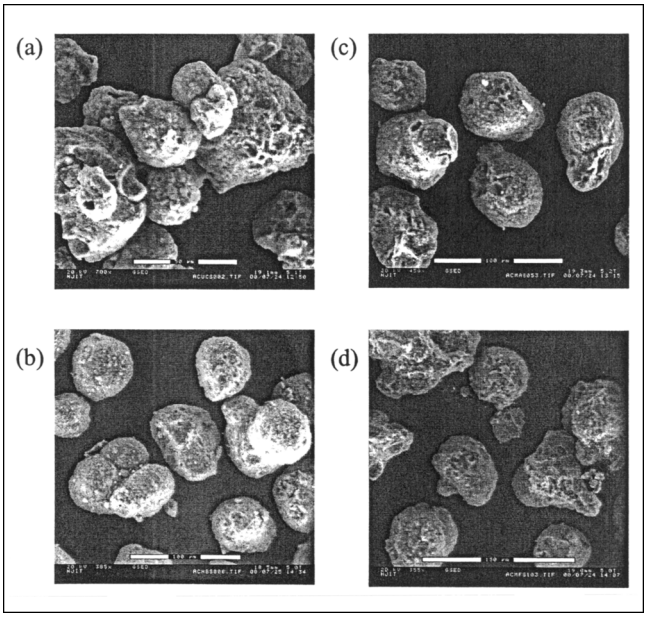

Figure 22. SEM micrographs of (a) uncoated, (b) HB-coated, (c) MAIC-coated, and (d) MF-coated samples, heated to 1,550°C in the dilatometer.

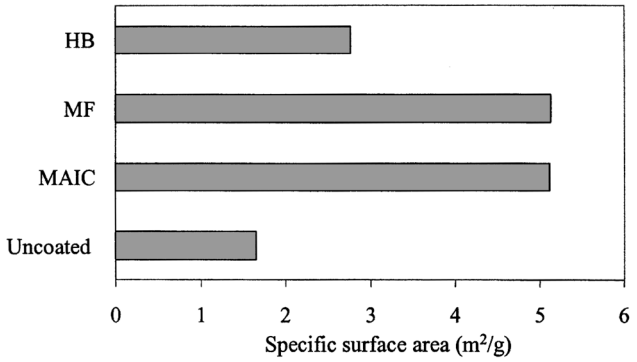

Figure 23. BET-specific surface area of samples heated to 1,550°C in the dilatometer.

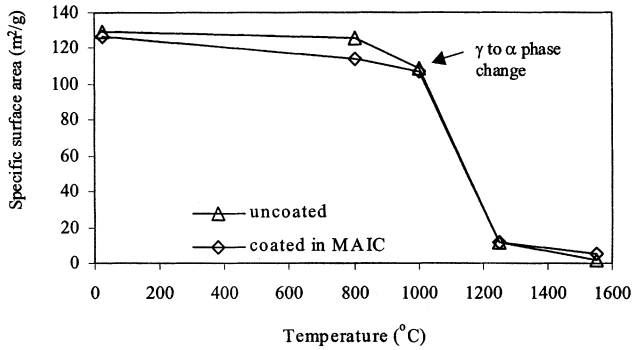

Figure 24. BET-specific surface area of uncoated and coated samples as a function of temperature.

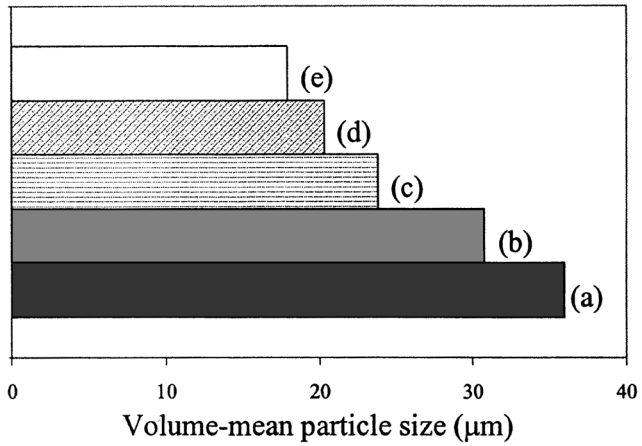

Figure 25. Volume–mean particle size of (a) uncoated alumina, (b) coated in MAIC for 2.5 min, (c) coated in MAIC for 5 min, (d) coated in MAIC for 10 min, and (e) coated in HB for 2 min (6,000 rpm).

The results of the sample processed for 2.5 min and the uncoated sample are presented in Figure 26. Both the coated and uncoated samples were heated to 1,250°C and 1,550°C. The dilatometry results of the samples heated to 1,550°C are shown in Figure 27. The minimum sintering temperature of the uncoated and the coated samples were found to be approximately 1,180°C and 1,320°C, respectively. SEM micrographs of the samples at 1,250°C are shown in Figures 28a and 28b. The SEM micrograph in Figure 28a shows an increase in neck growth of the uncoated sample at 1,250°C, whereas the coated sample remained as individual particles at 1,250°C in Figure 28b, agreeing with the dilatometry results.

Phenomenological Models of Deactivated Sintering

The mechanism of sintering can be due to volume diffusion and surface diffusion, viscous flow, and evaporation–condensation, as previously mentioned. These mechanisms are distinguished by the relationship of the radius of

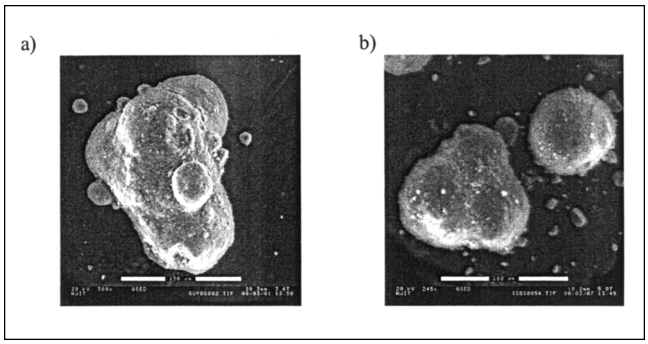

Figure 26. SEM micrographs of (a) alumina–silica uncoated, and (b) alumina silica coated for 2.5 min in MAIC, at room temperature.

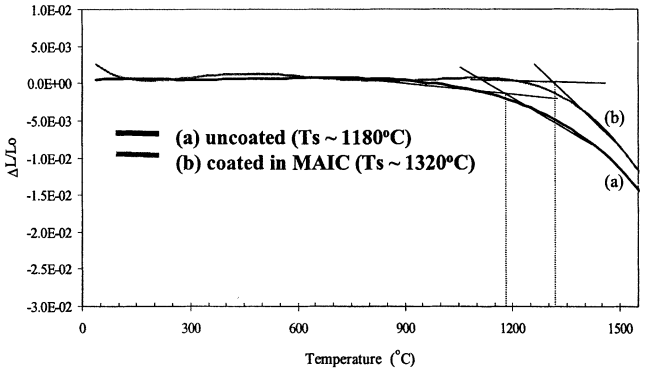

Figure 27. Elongation–contraction of uncoated and coated samples heated to 1,550°C in the dilatometer.

"neck" growth 2x (Figure 1) of two particles of the same size, as a function of time. These relationships have been discussed by numerous investigators and have been used to describe the sintering mechanism of different materials. The relationships are as follows (Kuczynski, 1949b)

$$\text{Viscous flow: } x^2 \sim t$$
$$\text{Evaporation–condensation: } x^3 \sim t$$
$$\text{Volume diffusion: } x^5 \sim t$$
$$\text{Surface diffusion: } x^7 \sim t.$$

Thus the rate of growth of the neck with time depends on which sintering mechanism is prevalent.

Alumina

For crystalline materials and metals the major sintering mechanism is volume diffusion (Coble, 1958). Thus, when two particles of approximately the same size are in contact, sintering depends on the concentration gradient between the curved neck region and the grain boundary. Based on the model of Kuczynski (1949a), where the volume diffusion mechanism of sintering was described using a vacancy concentration theory at the interface, the increase in vacancy concentration ΔC can be estimated from the Kelvin equation

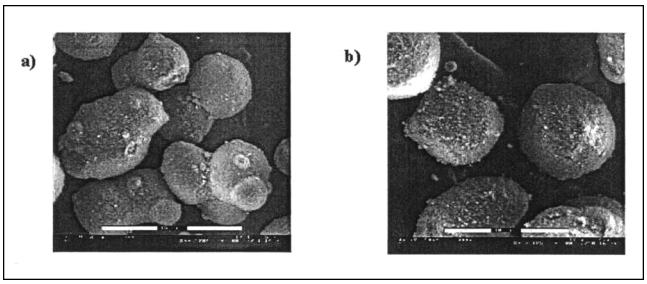

Figure 28. SEM micrographs of (a) uncoated alumina–silica and (b) alumina–silica coated in the MAIC for 2.5 min, heated to 1,250°C in the dilatometer.

as follows

$$\Delta C = \frac{\gamma C_0 \delta^3}{\kappa T}\left(\frac{1}{a} - \frac{1}{x}\right), \tag{4}$$

where C_0 is the equilibrium vacancy concentration, γ is the surface energy, δ^3 is the vacancy volume, x is the radius of the neck, a is the radius of the meniscus (see Figure 1), κ is the Boltzmann constant, and T is the absolute temperature. Since $x \gg a$, the equation reduces to

$$\Delta C = \frac{\gamma C_0 \delta^3}{\kappa T}\left(\frac{1}{a}\right). \tag{5}$$

As the uncoated alumina and the SiC-coated alumina undergo both neck growth and shrinkage, the volume of the host material arriving at the surface of the guest/host particles is given by (Coble, 1958)

$$\frac{dV}{dt} = \pi x^2 \frac{dy}{dt}, \tag{6}$$

where $y = x^2/4R$, and R is the radius of the host particle. The instantaneous mass flux, J, of the vacancies leaving the neck is given by Fick's first law

$$J = D_v A \frac{\Delta C}{x} \approx 4Dv\Delta C(2\pi x), \tag{7}$$

where D_v is the vacancy diffusivity for atoms, ions, or molecules of the host particles. Therefore, the volume diffused is given by

$$\frac{dV}{dt} = \frac{\pi x^3}{2R}\frac{dx}{dt} = J\delta^3 = 4D_v\Delta C(\pi x)\delta^3. \tag{8}$$

Equating the vacancy diffusivity, D_v, in Eq. 8, and the self-diffusion coefficient D_D, such that $C_0 D_v = D_D \delta^3$, and substituting $\Delta C = C_0(\gamma\delta^3/\kappa Ta)$ and $a = x^2/(4R)$ results in the following expression

$$\int x^4\, dx = \int \frac{64 D_D \gamma \delta^3}{\kappa T} R^2\, dt. \tag{9}$$

Integrating Eq. 9 results in the following expression

$$\left(\frac{x}{R}\right)^n = A\,\frac{D_D \gamma \delta^3}{R^3 \kappa T} t, \tag{10}$$

where $n = 5$, and A is a constant, and can be different depending on the mechanism of sintering (Coble, 1958). The sintering model can also be written in terms of the contraction of the sample as

$$\left(\frac{\Delta L}{L_0}\right)^p = B\,\frac{D_D \gamma \delta^3}{R^3 \kappa T} t, \tag{11}$$

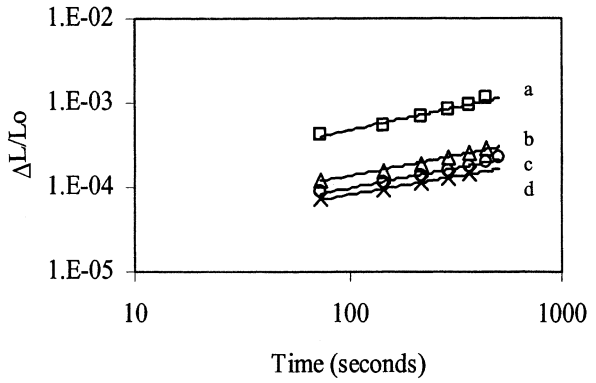

Figure 29. Contraction as a function of time at a temperature of 1,250°C for (a) uncoated alumina, (b) HB-coated sample (2 min, 6,000 rpm), (c) MAIC-coated sample (5 min), and (d) MF-coated sample (10 min, 600 rpm).

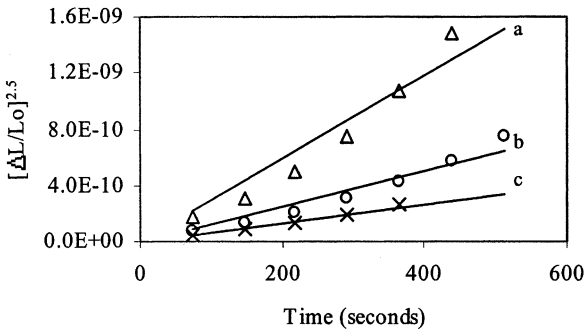

Figure 31. Contraction to the 2.5 power, as a function of time at an isothermal temperature of 1,250°C for alumina (a) MAIC-coated samples, (b) HB-coated samples, and (c) MF-coated samples.

where ΔL is the change in the length of the sample, L_0 is the initial length of the sample, $p = n/2$ is determined by the mechanism of sintering, and B is a constant. For volume diffusion $p = 2.5$.

Using our modified vertical dilatometer, $\Delta L/L_0$ can be directly measured as a function of time, isothermally. From these plots, an "effective" diffusivity of the uncoated and coated particles can be calculated. However, first it is necessary to verify that the primary mechanism of sintering is indeed volume diffusion. This is determined from a log plot of $\Delta L/L_0$ as a function of time, t, where the slope of the line determines $1/p$.

Plots of log $(\Delta L/L_0)$ as a function of log (t), for the uncoated and SiC-coated alumina processed in MAIC, mechanofusion, and the hybridizer, at 1,250°C, are shown in Figure 29. The slopes of all the lines were between 0.43 and 0.53 by a least-square fit. Taking into account experimental error, it seems reasonable to assume p to be approximately 2.5, indicating that the constant B is 10 (Coble, 1958), and that volume diffusion is indeed the predominant mechanism of sintering for alumina. The slope of $(\Delta L/L_0)^{2.5}$ as a function of time, t (see Figures 30 and 31), is used to calculate the effective diffusivity of the uncoated and the coated samples according to Eq. 10.

The effective diffusivities and the ratio of the diffusivity of the coated to uncoated samples are listed in Table 5. The table indicates that the effective diffusivity of the uncoated alumina (alumina–alumina system) is much higher than the coated material (alumina–SiC system). The lower diffusivity for the coated sample results in a reduction in the rate of sintering, which causes an increase in the sintering temperature of the material with a surface coverage of SiC. It should be noted that in all of the experiments, the time that the sample was maintained at a given constant temperature was always less than 10 min. The significance of this "dwell time" will be discussed in a subsequent article.

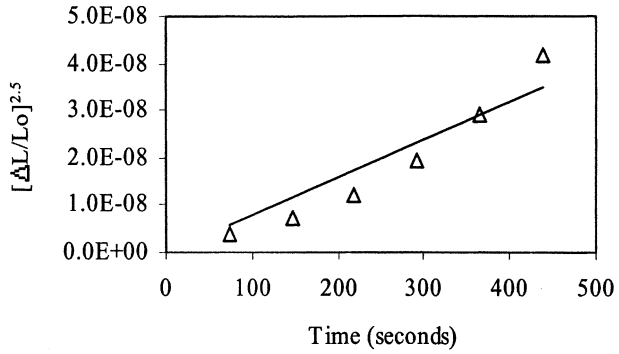

Figure 30. Contraction to the 2.5 power as a function of time, at an isothermal temperature of 1,250°C for uncoated alumina.

Glasses and polymeric materials

Frenkel (1945) presented a general expression for the neck growth between two similar-size spheres of the same material where viscous flow is the predominant mechanism of coating

$$\left(\frac{x}{R}\right)^2 = \frac{3\Gamma t}{2R\eta}, \tag{12}$$

where x is the neck growth, R is the radius of the particle, Γ is the effective surface energy of the two surfaces, t is the sintering time, and η is the viscosity coefficient.

Tardos et al. (1984) used a dilatometer to measure the effective viscosities of glass and polymers at temperatures close to the minimum sintering temperature. Their sintering model is briefly outlined below. The contraction of the sample can be expressed as a function of the radius of the sintered neck,

Table 5. Effective Diffusivity of Uncoated and Coated Samples

Sample	Diffusivity (cm^2/s)	Ratio
Uncoated high-purity γ-alumina	7.69×10^{-14}	1.000
MAIC-coated sample (5 min)	1.22×10^{-15}	0.016
HB-coated sample (2 min, 6,000 rpm)	8.11×10^{-16}	0.011
MF-coated sample (10 min, 600 rpm)	2.84×10^{-16}	0.004

x, by the following equation

$$\left[\frac{x}{D}\right]^2 \cong \left[f\,\frac{\Delta L}{2L_0}\right], \tag{13}$$

where ΔL is the contraction of the sample, L_0 is the initial length of the sample, D is the host particle diameter, and f is related to the layer spacing and the voidage of the arrangement of particles, such that for small particles

$$f = \frac{3\beta}{2} \tag{14}$$

and

$$\beta = \sqrt{\frac{2}{3}}\left[\frac{\pi}{3\sqrt{2}\,(1-\epsilon)}\right]^{1/3} \tag{15}$$

where β is the so-called layer spacing and ϵ is the porosity of the sample.

The general relationship between the size of the sinter neck, x, the compression force, F, the time, t, and the effective viscosity of the host particle, η_s, neglecting any compression force due to surface tension and van der Waals forces (see Rumpf, 1977) can be expressed by the following equation, where $K = 2/5\pi$ and $n = 1$ for viscous flow

$$\left[\frac{b}{D}\right]^2 = \left[\frac{KF\,t}{D^2\eta_s}\right]^n. \tag{16}$$

Using Eq. 13 to replace the neck radius by the contraction, we obtain:

$$f\left(\frac{\Delta L}{2L_0}\right) = \left[\frac{KFt}{D^2\eta_s}\right]^n. \tag{17}$$

Using data from the dilatometer at a constant temperature, a log plot of the change in contraction of the sample $f(\Delta L/2L_0)$ is plotted against time, t. Provided that the slope, n, of this relationship is 1, indicating that the sintering mechanism is indeed viscous flow, Eq. 17 can be reduced to

$$\eta_s = \frac{KF\,D^{-2}}{\dfrac{\left(f\,\dfrac{\Delta L}{2L_0}\right)}{t}}. \tag{18}$$

The compression force, F, applied to the sample in the dilatometer is related to the load applied to the piston by

$$F = \frac{4\epsilon(D)^2 L}{\left[\pi(1-\epsilon)(D_s)^2\right]}. \tag{19}$$

The load, L, used for all the experiments was 35 g, and the diameter, D_s, of the sample tube was 4 mm. The porosity, ϵ, used for the calculations was 0.4, resulting in a value of 1.31 for f.

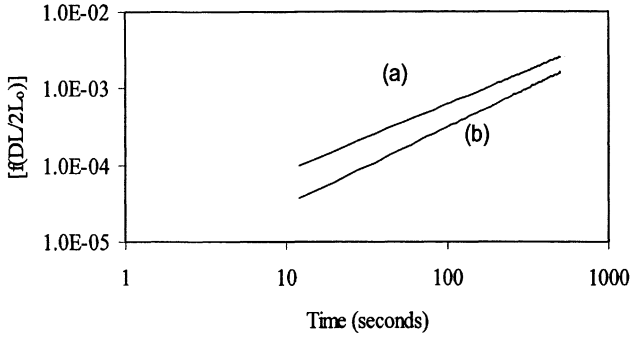

Figure 32. Log plot of contraction as a function of time at 620°C for (a) uncoated glass beads, and (b) glass beads coated with 8 wt. % of SiC (40 data points used for each plot).

Equations 17 and 18 were used to calculate the effective viscosity of the uncoated and the coated materials, for both glass beads and PMMA. This calculation is based on the assumption that the mechanism of sintering, with and without a surface coating, is due to viscous flow. A log plot of $f(\Delta L/2L_0)$ against time, t, for glass beads, uncoated and coated with 8 wt % SiC in the MAIC, at an isothermal temperature of 620°C, is shown in Figure 32. The slope, n, for the uncoated and the coated samples is found to be 0.87 and 1.01, respectively, close enough to unity if experimental error is taken into account. This indicates that Eq. 18 can be used to calculate the effective viscosity of both the uncoated and coated samples. It is clear that the intrinsic viscosity of the glass beads at a given temperature should not change. However, the amount of coverage of SiC on the surface of the beads, affects the viscous flow mechanism, resulting in a higher "effective" viscosity.

An arithmetic plot of the contraction as a function of time at an isothermal temperature of 620°C, for the uncoated and coated samples, is shown in Figure 33. The slope of the curve for the uncoated sample is greater than the slope for the coated sample, indicating that the effective viscosity of the coated sample is higher than the uncoated sample. Similar plots (not shown) were also constructed from dilatometry data

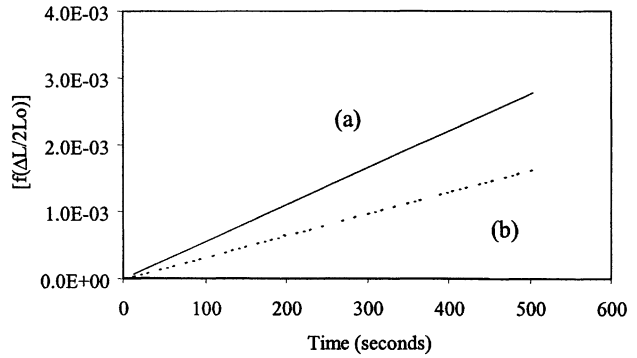

Figure 33. Arithmetic plot of contraction as a function of time at 620°C for (a) uncoated glass beads, and (b) glass beads coated with 8 wt. % of SiC (40 data points used for each plot).

Table 6. Effective Viscosity of Coated and Uncoated Samples at Different Temperatures

		Effective Viscosity (Pa·s)		Ratio Coated/ Uncoated
		Uncoated	Coated	
Glassbeads	600°C	6.93×10^9	9.53×10^9	1.4
	620°C	4.67×10^9	7.62×10^9	1.7
PMMA	105°C	0.93×10^9	1.97×10^9	2.1
	120°C	0.56×10^9	1.79×10^9	3.2

for glass beads, uncoated and coated, for an isothermal temperature of 600°C. Plots were also constructed from data obtained for PMMA, uncoated and coated in the MAIC for 5 min with 3 wt % SiC, at two isothermal temperatures of 105 and 120°C. The slope, n, from the log plot of $[f(\Delta L/2L_0)]$ as a function of time, t (not shown), yielded values between 0.80 and 1.20, again indicating that viscous flow is the dominant mechanism of sintering.

The effective viscosity of the glass beads and PMMA, and the ratio of the viscosity of the coated material to the uncoated material at each temperature, are given in Table 6. In all cases the effective viscosity of the coated particles is higher than that of the uncoated particles. This is due to the discrete coating of SiC that slows the sintering mechanism, by retarding the viscous flow of the glass and PMMA material toward the neck area, promoting deactivated sintering.

Conclusions

The phenomenon of deactivated sintering has been successfully demonstrated by applying a discrete coating of SiC onto the surface of a variety of host powders using dry-particle coating. It was possible to obtain individual particles of PMMA at 150°C, about 45°C above the minimum sintering temperature ($T_s \sim 105$°C) of the uncoated PMMA with a surface coating of SiC using all three dry-coating devices. At this temperature, uncoated PMMA particles were totally sintered. For glass-bead samples coated with 0.8 wt % SiC it was also possible to obtain individual particles of coated glass beads at 700°C, about 125°C above the minimum sintering temperature ($T_s \sim 575$°C) of uncoated glass beads. With the use of 8 wt % of SiC, it was possible to obtain individual particles even at 800°C. Thus, an increase in deactivated sintering is observed with an increase in guest weight (greater surface coverage).

For the high-purity γ-alumina we also observed an increase in the sintering temperature when coated with SiC. However, a phase change from γ to α was obtained at around 1,000°C. Thus, this material loses its desirable high surface area at temperatures below the minimum sintering temperature.

The alumina–silica catalyst support material underwent various degrees of attrition when processed in all three dry-particle coating devices. Based on changes in the volume–mean particle size of the samples after processing, the least attrition was observed using MAIC processing for 2.5 min. Even for this short processing time, however, an increase in sintering temperature of the coated sample of almost 140°C was observed. SEM micrographs clearly supported the dilatometry studies.

A phenomenological model of deactivated sintering for both crystalline (alumina) and amorphous (glass and polymers) materials was investigated using the experimental dilatometry data. For crystalline materials, it was found that the neck growth and shrinkage of the material was due primarily to volume diffusion as previously reported in the literature. The application of a discrete surface coating of SiC on the alumina particles provides a deactivated layer. This deactivated layer causes a significant reduction in the effective diffusivity of the coated material, resulting in a delay in the sintering of the material and an increase in the minimum sintering temperature.

For amorphous (glass and polymers) materials, the mechanism of sintering was primarily due to viscous flow of the host material. The deactivated layer of SiC on the surface of glass beads and PMMA caused an increase in the effective viscosity of the material. The effective viscosity of the coated material was 1.5 times larger than the uncoated material for glass beads and more than two times larger than the uncoated PMMA. The increase in the effective viscosity is caused by the surface coverage of the SiC retarding the flow of the softened PMMA or glass, resulting in a delay in the sintering of the material and an increase in the minimum sintering temperature.

Acknowledgments

The authors gratefully acknowledge the National Science Foundation under Grant CTS-9985618 and the New Jersey Commission on Science and Technology (01-2042-007-24 and 97-100-020-2890-051-6130) for supporting this research.

Literature Cited

Alonso, M., M. Satoh, and K. Miyanami, "Powder Coating in a Rotary Mixer with Rocking Motion," *Powder Technol*., **56**, 135 (1988).

Alonso, M., M. Satoh, and K. Miyanami, "Mechanism of Combined Coating Mechanofusion Processing of Powders," *Powder Technol*., **59**, 45 (1989a).

Alonso, M., M. Satoh, and K. Miyanami, "Kinetics of Fines Transfer Among Carriers in Powder Coating," *Powder Technol*., **59**, 217 (1989b).

Bonis, L. J., and H. H. Hausner, eds., *Sintering and Plastic Deformation, Proceedings*, Plenum Press, New York (1964).

Coble, R. I., "Initial Sintering of Alumina and Hematite," *J. Amer. Ceram. Soc*., **41**, 55 (1958).

Coble, R. I., "Sintering Crystalline Solids I: Intermediate and Final State Diffusion Models," *J. Appl. Phys*., **32**, 787 (1961).

Compo, P., G. I. Tardos, D. Mazzone, and R. Pfeffer, "Minimum Sintering Temperatures of Fluidizable Particles," *Part. Character. I*, 171 (1984).

Compo, P., R. Pfeffer, and G. I. Tardos, "Minimum Sintering Temperatures and Defluidization Characteristics of Fluidizable Particles," *Powder Technol*., **51**, 85 (1987).

Frenkel, J., *J. Phys*. (*U.S.S.R.*), **9**, 385 (1945).

German, R. M., *Powder Metallurgy Science*, Metal Powder Industries Federation (1984).

Hendrickson, W., and J. Abbott, "Process for Making Particle-Coated Solid Substrates," U.S. Patent No. 5,962,082 (1997).

Honda, H., M. Kimura, T. Matsuno, and M. Koishi, "Preparation of Composite and Encapsulated Powder Particles by Dry Impact Blending," *CHIMICA OGGI: Int. J. Chem. Biotechnol.*, **9**, 21 (1991).

Honda, H., M. Kimura, F. Honda, T. Matsuno, and M. Koishi, "Preparation of Monolayer Particle Coated Powder by the Dry Impact Blending Process Utilizing Mechanochemical Treatment," *Colloids Surface A: PhysicoChem. Eng. Aspects*, **82**, 117 (1994).

Houdayer, A., G. Cerny, J. E. Klemberg-Sapieha, G. Czeremuszkin, and M. R. Wertheimer, "MeV Proton Irradiations and Atomic

Oxygen Exposure of Spacecraft Materials with SiO_2 Protective Coatings," *Nucl. Instrum. Methods Phys. Res. B*, **131**, 335 (1997).
Ishizaka, T., H. Honda, Y. Kikuchi, T. Katano, and M. Koishi, "Preparation of Drug-Diluent Hybrid Powders by Dry Processing," *Chem. Pharm. Bull.*, **36**, 2562 (1988).
Johnson, J. L., and R. M. German, "Theoretical Modeling of Densification During Activated Solid-State Sintering," *Metall. Mater. Trans. A*, **27A**, 441 (1996).
Kuczynski, G. C., "Self-Diffusion in Sintering of Metallic Particles," *Trans. AIME*, **185**, 169 (1949a).
Kuczynski, G. C., "Study of the Sintering of Glass," *J. Appl. Phys.*, **20**, 1160 (1949b).
Lide, D. R., ed., *CRC Handbook of Chemistry and Physics*, 79th ed., Boca Raton, FL (1998–1999).
Luo, J., H. Wang, and Y.-M. Chaing, "Origin of Solid-State Activated Sintering in Bi_2O_3-Doped ZnO," *J. Amer. Ceram. Soc.*, **82**, 916 (1999).
Naito, M., A. Kondo, and T. Yokoyama, "Application of Comminution Techniques for the Surface Modification of Powder Materials," *ISIJ Int.*, **33**, 915 (1993).
Panin, V. E., A. I. Slosman, and S. V. Matrenin, "Activated Sintering of Zirconium Dioxide," *Russ. Phys. J.*, **39**, 160 (1996).
Pfeffer, R., R. N. Dave, D. Wei, and M. Ramlakhan, "Synthesis of Engineered Particulates with Tailored Properties Using Dry Particle Coating," *Powder Technol.*, **117**, 49 (2001).
Ramlakhan, M., R. N. Dave, and R. Pfeffer, "Dry Particle Coating Using Magnetically Assisted Impaction Coating: Modification of Surface Properties and Optimization of System and Operating Parameters," *Powder Technol.*, **112**, 137 (2000).
Rumpf, H., "Particle Adhesion," *Agglomeration 77*, K. V. S. Sastry, ed., AIME, New York, p. 97 (1977).
Siegell, J. H., "High-Temperature Defluidization," *Powder Technol.*, **38**, 13 (1984).
Singh, R. K., A. Ata, J. Fitz-Gerald, Y. I. Rabinovich, and W. Hendrickson, "Dry Coating Method Using Magnetically Assisted Impaction in a Random Turbulent Fluidized Bed," *KONA*, **15**, 121 (1997).
Tanno, K., "Current Status of the Mechanofusion Process for Producing Composite Particles," *KONA*, **8**, 74 (1990).
Tardos, G., D. M. Mazzone, and R. Pfeffer, "Measurement of Surface Viscosities Using a Dilatometer," *Can. J. Chem. Eng.*, **62**, 884 (1984).
Watano, S., Y. Imada, K. Miyannami, C. Y. Wu, R. N. Dave, R. Pfeffer, and T. Yoshida, "Surface Modification of Food Fiber by Dry Particle Coating," *J. Chem. Eng. Jpn.*, **33**, 848 (2000).
Yokoyama, T., K. Urayama, M. Naito, M. Kato, and T. Yokoyama, "The Angmill Mechanofusion System and Its Application," *KONA*, **5**, 59 (1987).

Manuscript received Apr. 30, 2002, and revision received Aug. 27, 2002.